Development and Analysis of a Waffle Constrained Reconstructor (WCR) for Fried Geometry Adaptive Optics Systems

Robert W. Praus, II
MZA Associates Corporation

ABSTRACT

A common difficulty of Fried-geometry adaptive optics (AO) is the build-up of the unsensed spatial wavefront mode called waffle. This paper presents the derivation of a Fried-geometry wavefront reconstructor matrix which ameliorates the impact of the waffle mode in closed-loop AO systems. Typical waffle suppression algorithms employ spatial filters that may adversely affect the AO system's ability to correct the highest spatial frequencies. Because it is not based on spatial filtering techniques, but on algebraic constraints in the development of the reconstructor matrix itself, the waffle constrained reconstructor may reduce the extent to which the correction of high spatial frequencies must be sacrificed in order to reduce waffle.

This paper provides the mathematical development of the waffle constrained reconstructor (WCR) and, through the use of wave-optics simulations, provides analysis of its closed-loop performance as compared to other reconstructors.

1. BACKGROUND

In a well-aligned Fried-geometry wavefront control (WFC) system [1] that employs a Shack-Hartmann wavefront sensor (WFS), the spatial wavefront phase mode called waffle [2] is unsensed by the WFS. While the natural occurrence of the waffle mode in aberrating media to be compensated is rare, it is very common for the mode to be imposed on the deformable mirror (DM) corrector through the propagation of errors in the sensing and control scheme. Left unchecked, waffle can build up on the DM and degrade the performance of the adaptive optics (AO) system. To ameliorate the problem, a number of approaches, most of which are implemented through modification of the WFC reconstructor matrix, have been proposed or implemented. Here we develop and analyze through simulation an approach based on algebraic constraints through a modification of the standard least-squares reconstructor formulation.

A Shack-Hartmann wavefront sensor consists of a plurality of subapertures covering the full pupil over which the wavefront measurement is to be made. The simple geometry of a single wavefront subaperture projected onto the DM is shown in Fig. 1. In a Fried-geometry configuration the corners, c_i, of the subaperture coincide with the location of discrete actuators of the DM and the slope of the wavefront of the portion of light between the actuators imaged by the subaperture can be estimated by spot displacements in x and y in the WFS image plane. The actuators can be displaced in corresponding amounts d_i, to redirect that portion of light so that it is centered in the wavefront sensor image plane.

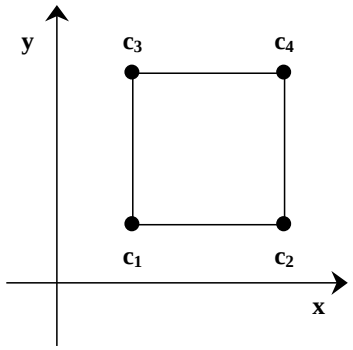

Fig. 1. Single Subaperture Geometry

Given displacements, d_i, of the actuators at c_i, the wavefront slopes, s_x and s_y, across the subaperture are reasonably approximated by

$$s_x = -d_1 + d_2 - d_3 + d_4 \quad (1)$$

$$s_y = -d_1 - d_2 + d_3 + d_4 \quad (2)$$

The approximations of equations (1) and (2) are commonly used for the construction of DM actuator slope influence functions to compute reconstructor matrices. Slope influence functions may also developed using more rigorous modeling of the DM actuator slope influence functions as well as through the direct measurement of the effects of actuator pokes on WFS subapertures. In some systems, it has been found that reconstructors derived from simple analytic influence functions that include the approximations of equations (1) and (2) work better than those derived by more rigorous modeling or measurement because the resulting reconstructors are better numerically conditioned. Nonetheless, the analysis presented herein is not dependent on the approximation. Other derivations of the WCR which include the more rigorous modeling or measurement techniques are possible.

Fig. 2 is a diagram large Fried-Geometry configuration showing the positions of actuators and subapertures as superposed on the pupil of a large telescope[1].

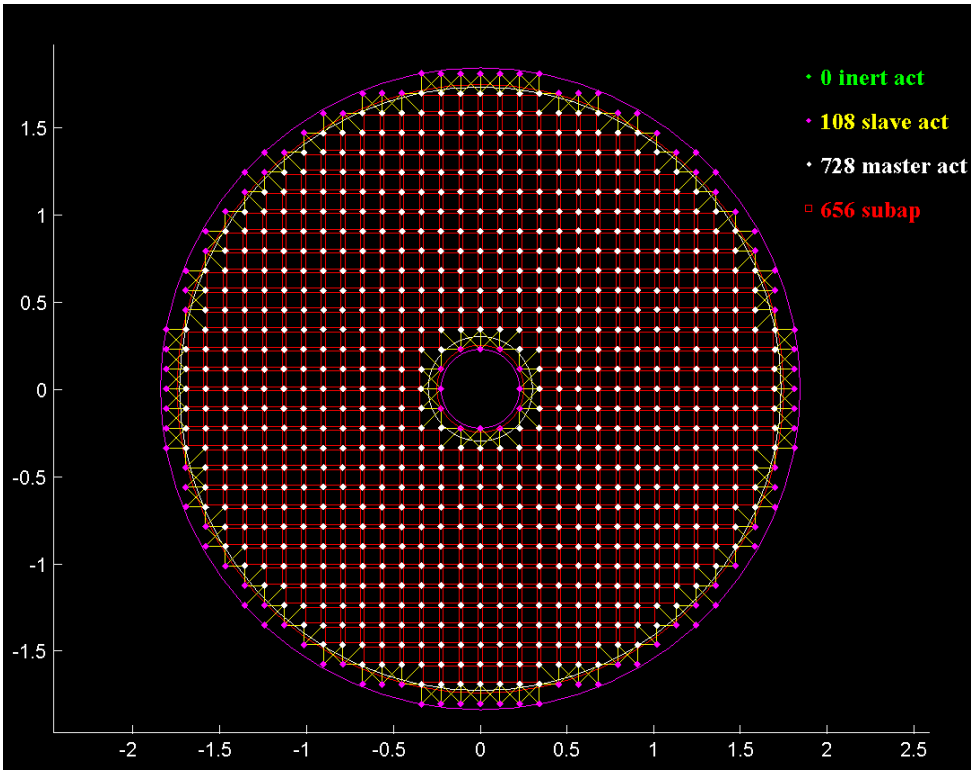

Fig. 2. A Large Fried-Geometry Adaptive Optics Layout

Because adjacent subapertures share actuators, solving for the best set of all actuator displacements becomes an over-constrained multiple-input-multiple-output (MIMO) feedback problem. This is typically accomplished in a least-squares fashion. The approach is to first use equations (1) and (2) and subaperture adjacency constraints to formulate the matrix A satisfying the equation

$$\mathbf{s} = A\mathbf{d} \quad (3)$$

[1] The inert and slave actuators referenced in Fig. 2 are not relevant to this discussion, but the slaves are shown because the configuration is used in subsequent simulation analysis.

where, **s** is the ordered x and y slopes across the subapertures resulting from actuator displacements **d** located at the corners of subapertures. What is usually desired is a reconstructor matrix which, given measured slopes across subapertures, provides displacements, $\mathbf{d}_{est}$, at the corners that can be used to best conjugate the indicated wavefront error while minimizing the square error. These displacements are then used in a feedback control loop to drive the actuators. The reconstructor is usually found by computing a pseudo-inverse of A, giving the equation

$$\mathbf{d}_{est} = A^{\#}\mathbf{s} \tag{4}$$

The pseudo inverse may be calculated in a variety of fashions, but usually singular value decomposition (SVD) techniques [3], [4], are used to obtain a system that minimizes the square error while suppressing the noise propagation of nearly-unsensed (i.e., singular) modes. Unfortunately, waffle is not typically a natural mode of the matrix and is not adequately suppressed by SVD conditioning.

2. DERIVATION

In a single subaperture, waffle is the spatial mode induced by pushing up equally on the one pair of corner actuators diagonal from each other, for example, c_1 and c_4, while simultaneously pulling down by the same amount on the other pair of diagonal actuators, c_2 and c_3. For such conditions, s_x and s_y of equations 1 and 2, compute to zero and the effect of the actuator displacements are unsensed by the wavefront sensor[2]. Equation 3 can be modified to constrain waffle by incorporating the single subaperture waffle equation

$$w = d_1 - d_2 - d_3 + d_4 \tag{5}$$

Using an approach similar to that used to formulate A, waffle can be combined with the subaperture slopes equations to create a matrix B, that generates a vector, **t**, containing both subaperture slopes and waffle components resulting from displacements at the actuators,

$$\mathbf{t} = \begin{bmatrix} \mathbf{s}_x \\ \mathbf{s}_y \\ \mathbf{w} \end{bmatrix} = \begin{bmatrix} [A_x] \\ [A_y] \\ [A_w] \end{bmatrix} \mathbf{d} = B\mathbf{d} \tag{6}$$

Here, A_x, A_y, and A_w are those portions of the matrix that relate to x slope, y slope, and waffle respectively. $\mathbf{s_x}$, $\mathbf{s_y}$, and **w** are subvectors of **t** containing the x and y slopes and waffle components for each subaperture. As before, this system gives rise to a reconstructor by taking the pseudo-inverse

$$\mathbf{d}_{est} = B^{\#}\mathbf{t} \tag{7}$$

But then **t** must contain both slope and waffle measurements. Since the reason that we wish to constrain waffle is that it is an unsensed mode (or at least nearly so), a scheme requiring a measurement of waffle would be silly. However, we are not really after a measurement of waffle, we are after a reconstructor that provides sets of displacements having no waffle. Breaking out the constituents of equation (7) further we get

$$\mathbf{d}_{est} = \begin{bmatrix} [B_x^{\#}] & [B_y^{\#}] & [B_w^{\#}] \end{bmatrix} \begin{bmatrix} \mathbf{s}_x \\ \mathbf{s}_y \\ \mathbf{w} \end{bmatrix} = B^{\#}\mathbf{t} \tag{8}$$

[2] Given the limitations of optical hardware and misalignments thereof, it is rare for an actual system to give rise to precisely equal actuator displacements or precisely zero measured slopes. However these conditions do occur approximately and are amenable to this analysis.

$B^{\#}$ is comprised of three components, $B_x^{\#}$, $B_y^{\#}$, and $B_w^{\#}$. To reconstruct a set of displacements representative of slopes $\mathbf{s}_x$ and $\mathbf{s}_y$, while minimizing waffle in a constrained least-squares sense, set $\mathbf{w}$ to zero and eliminate $B_w^{\#}$ and $\mathbf{w}$ from the equation altogether. Hence there is no need for a waffle measurement and the following is obtained,

$$\mathbf{d}_{\text{est}} = \begin{bmatrix} B_x^{\#} \end{bmatrix} \begin{bmatrix} B_y^{\#} \end{bmatrix} \begin{bmatrix} \mathbf{s}_x \\ \mathbf{s}_y \end{bmatrix} = C^{\#}\mathbf{s} \tag{9}$$

$C^{\#}$ is the waffle constrained reconstructor (WCR) matrix formed by removing the waffle-related columns of $B^{\#}$ obtained from a pseudo-inverse of a simple set of equations containing the waffle component equations.

3. SIMULATION

To evaluate the relative performance of different reconstructors, a WaveTrain wave-optics model [5] of the Starfire Optical Range (SOR) 3.5 meter telescope as it existed in the late 1990's was resurrected. The specifications of the SOR system were derived from [6] in which the performance of the system was evaluated for astronomical viewing. A description of the model that provides results consistent with those presented herein appears in [7].

Fig. 3 is the top-level WaveTrain diagram of the model used in this study. The model implements closed-loop AO and track systems using a standard tip-tilt centroid tracker and a tilt-removed least-squares reconstructor of a Fried-geometry Shack-Hartmann wavefront sensor. Both the track and WFS cameras image an idealized point source from the target astronomical object. The system also contains a "science" camera which images the target astronomical object, in this case, two point sources separated by 0.3 arc seconds representing the k-Peg binary star system, that conveniently happen to be centered on the AO and track beacon. A compensated Gaussian beam is back-propagated through the shared aperture and sampled by a target board at the target to simulate the performance of a compensated shared-aperture illuminator.

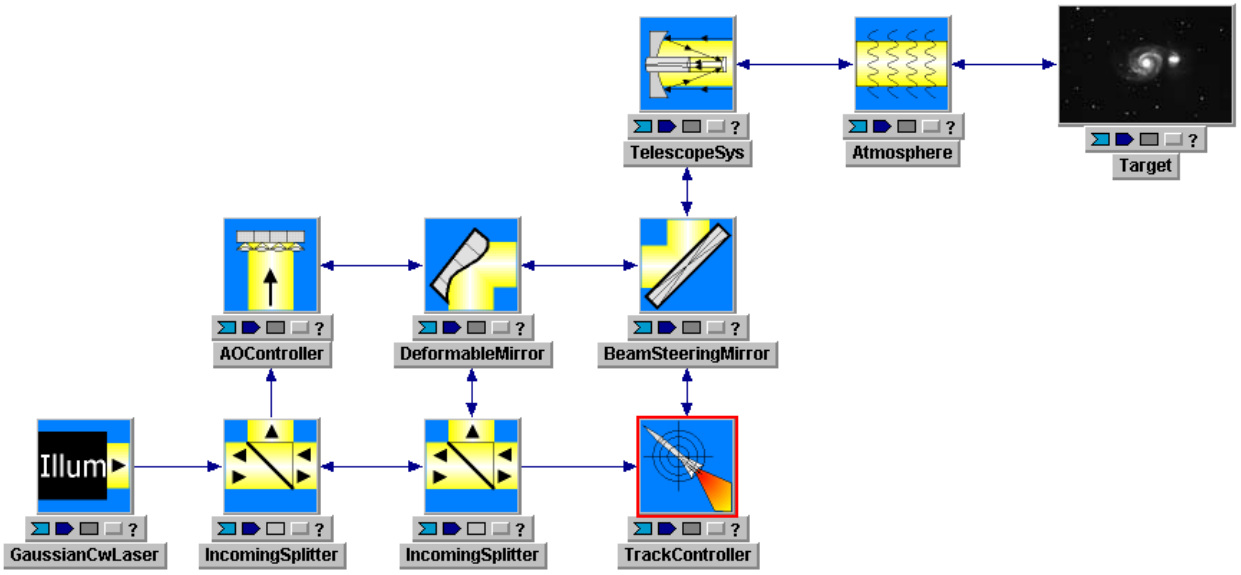

Fig. 3. The Top-Level WaveTrain Diagram of the SOR Model Employed in this Study

The model contains the fundamental characteristics of the SOR 3.5 meter telescope. The AO system uses a 30 x 30 subaperture Fried-geometry wavefront sensor to drive a DM containing 728 master actuators with 108 slaved actuators at the edges (Fig. 2). The track and AO control loops are sampled at 1,500 frames per second and have been characterized to have closed-loop -3 db cross-over frequencies of approximately 160 Hz[3]. The track system is very highly resolved and has zero camera noise to facilitate the detailed study of the AO system without worrying about interaction with the track loop.

[3] 160 Hz is possible with 1,500 samples per second because the control loops were implemented with zero latency. These bandwidths were chosen to be representative of what might be implemented in an actual system.

4. RESULTS

The wave-optics simulation was used to evaluate the performance of the WCR as compared to a standard SVD-conditioned pseudo-inverse reconstructor, and a reconstructor that uses a spatial filtering form of waffle suppression [8]. Reference [8] is an analysis of the use of spatial filtering techniques to increase the stability margin of an AO control system by reducing the propagation of measurement error. From [8], the noise gain, G_R, of the reconstructor R is defined as

$$G_R = 1/N \text{ Trace}(RR^T) \tag{10}$$

where, N is the number of actuators. Table 1 describes the reconstructors compared in this study.

Table 1. Descriptions of the Reconstructors Compared in the Study

Symbol & Name	Description	Noise Gain
S Standard	A standard tilt-removed reconstructor computed using the method described for $A^{\#}$ in Section 1. Two singular values were removed in SVD processing.	0.0050
T T-Filter	The reconstructor formed by pre-multiplying S by the convolution T-filter as described in [8].	0.0016
W WCR	A tilt-removed Waffle Constrained Reconstructor derived like $C^{\#}$ in Section 2. A single singular value was removed in SVD processing.	0.0023

A set of parameterized runs was used to evaluate the time-averaged performance of the AO system for each of the three reconstructors. Specifically, the runs varied the turbulence strength by factors of 1, 2, 3, and 4 times Clear-1 Night profile [9] and the WFS camera read noise such that the standard deviation of the noise was approximately 0.05, 0.1, 0.25, and 0.3 times the maximum signal of a well-compensated system.

For a 2 x Clear-1 Night atmosphere with a uniform effective wind of 7 m/s, Fig. 4 shows instantaneous intensity-normalized images of the science camera that images the astronomical target at 6.4 μm for both uncompensated and compensated cases.

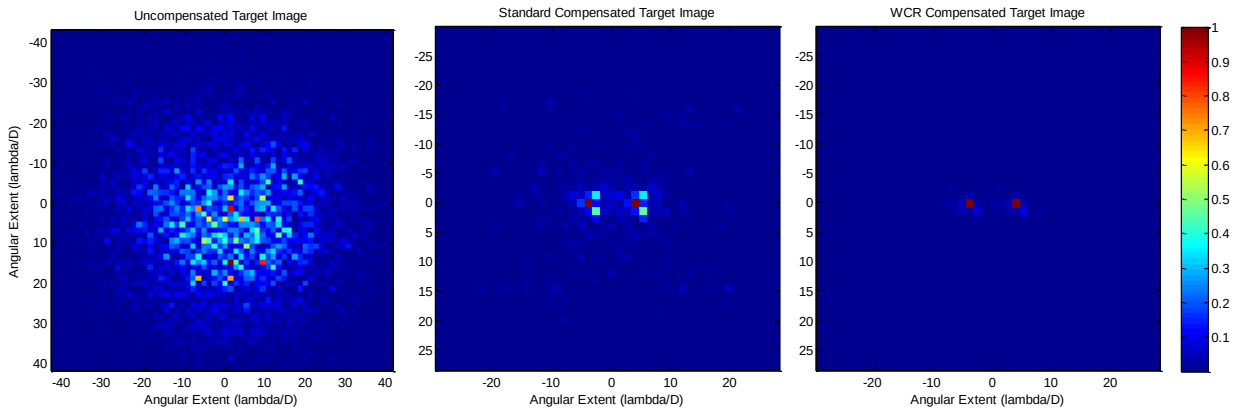

Fig. 4. Instantaneous Target Imaged a 2 x Clear-1 Night Atmosphere with a Uniform 7 m/s Wind

In this case, the WCR provides better compensation, but is the improvement due, at least in part, to the suppression of waffle? Fig. 5 shows normalized sums of the pixels transverse to the target object source separation of the long-term averaged image plane for the 2 x Clear-1 Night case. The locations of the separated target object sources are roughly at -5 and +5 times λ/D and correspond to the peaks of the compensated cases. For the Standard compensation case, there are secondary peaks approximately 15 λ/D from the primary peaks. The location of the secondary peaks correspond to the spatial frequency of the waffle mode which is λ divided by twice the actuator spacing. At least some of the high-spatial frequency content in the Standard reconstructor image plane is consistent with the build-up of waffle.

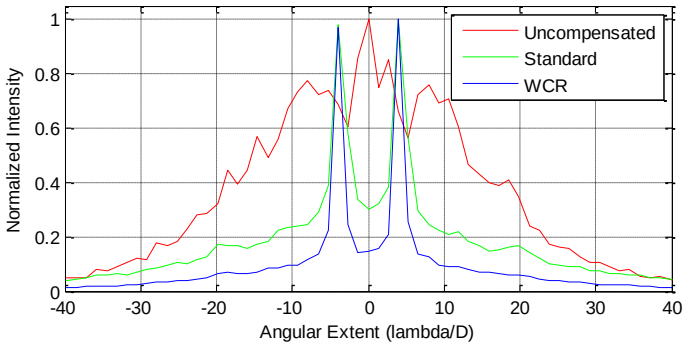

Fig. 5. Normalized Transverse Sums of the Long-Term Averaged Image Plane for the 2 x Clear-1 Night Case

Fig. 6 shows instantaneous actuator displacements resulting from AO control using the Standard and WCR reconstructors for the 2 x Clear-1 Night case. Waffle mode is clearly present in the Standard reconstructor case and is not apparent in the WCR.

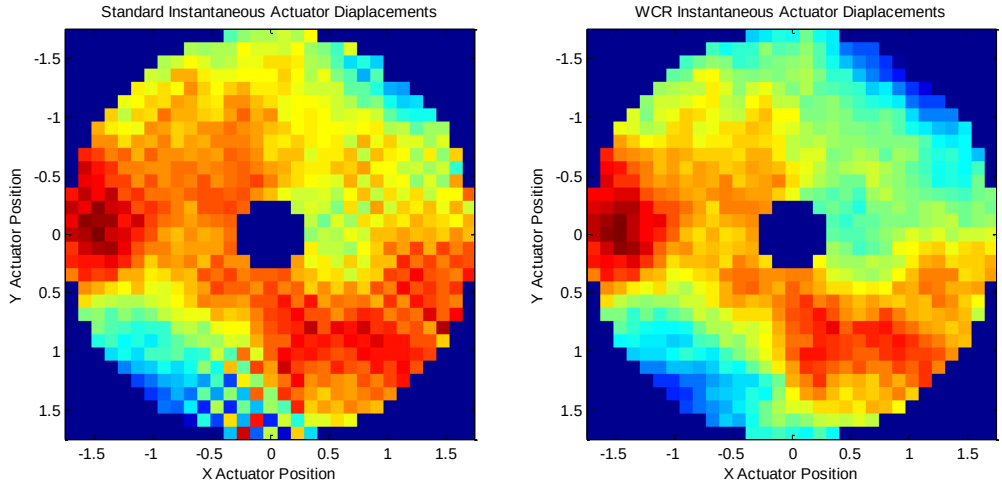

Fig. 6. Instantaneous Actuator Displacements

The remaining results are provided as a series of comparative plots for various performance metrics. Ignoring transmission losses, Fig. 7 shows the time-averaged normalized peak intensity as received by the highly resolved track camera that images an idealized point source beacon for each reconstructor, the indicated noise levels, and turbulence multipliers. The color scale of Fig. 7 is normalized to the peak intensity of the sensor when the beacon is imaged through a vacuum. Fig. 8 is the same data as in Fig. 7 but shown as the ratio of the WCR results to the results of the Standard and T-Filter reconstructors. Because the present study is concerned with comparisons of the WCR with the other reconstructors, the rest of the parametric results will be presented in this format. For the most part, all the metrics had the same sort of relative performance as compared to the idealized vacuum case. For low-turbulence conditions the compensated cases provided factors of 0.25 - 0.4 times performance of the idealized case and for the high-turbulence cases, compensation resulted in less than 0.02 times the performance. Fig. 9 is the comparative time-averaged on-axis intensities from the track camera. Fig. 10 is the comparative time-averaged encircled energy in a 4λ/D bucket in the track camera.

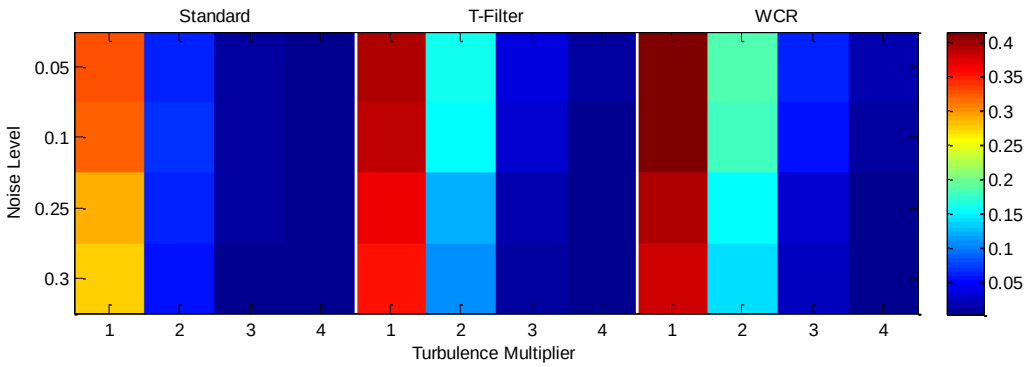

Fig. 7. The Time-Averaged Normalized Peak Intensity in the Track Camera

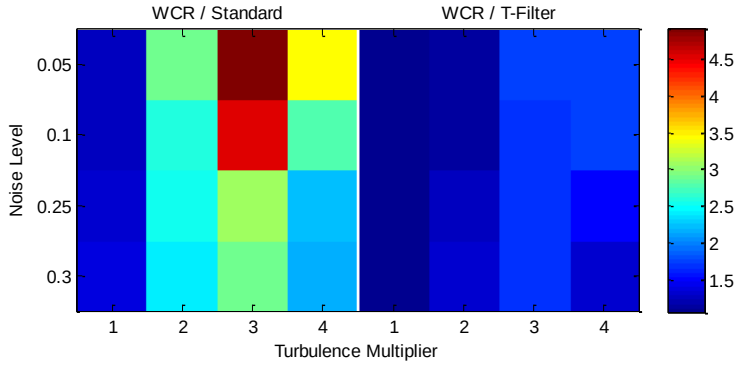

Fig. 8. The Comparative Time-Averaged Peak Intensity in the Track Camera

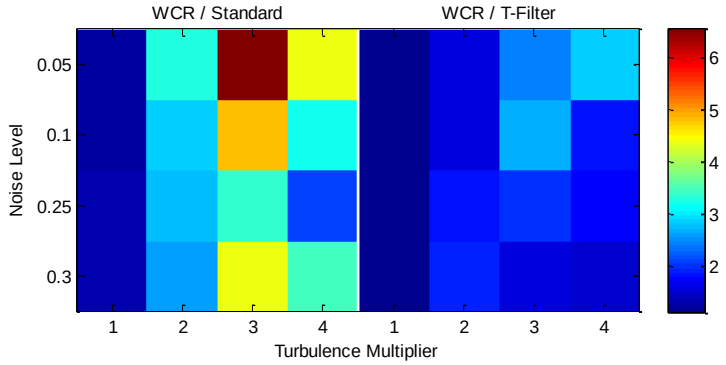

Fig. 9. The Comparative Time-Averaged On-Axis Intensity in the Track Camera

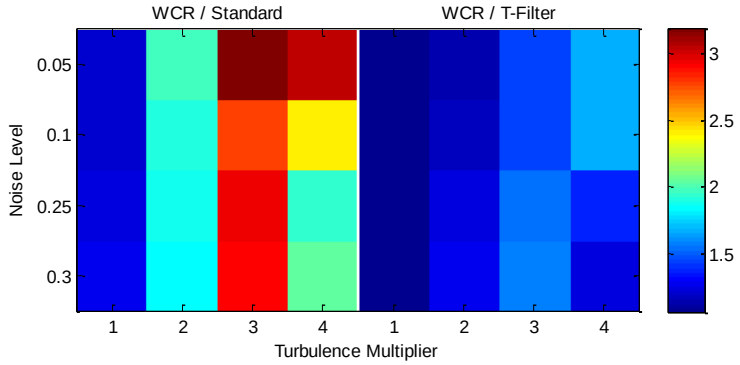

Fig. 10. The Comparative Time-Averaged Encircled Energy in a 4λ/D Bucket in the Track Camera

Fig. 11 presents the comparative contrast visibility of time-averaged image of the target object. The contrast visibility was computed as the mean of the intensities of the two peak pixels corresponding to the two sources divided by the mean of the intensities on the pixels in between the two peaks.

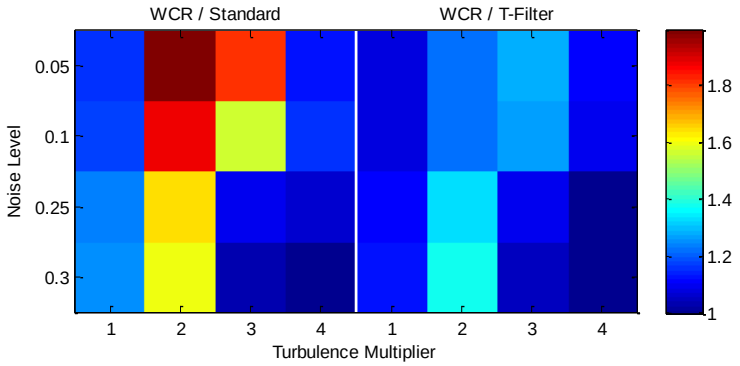

Fig. 11. The Comparative Contrast Visibility of the Time-Averaged Image of the Target Object

5. CONCLUSION

From the results, we can conclude that the WCR provides improved performance over the Standard and T-Filter reconstructors. For most metrics, WCR improves performance less for the weak-turbulence cases than for the stronger turbulence cases. The improvement of WCR over the T-Filter was less than for the Standard reconstructor.

This study is not comprehensive and does not take into account numerous issues that further complicate Fried-geometry AO control. Specifically, the performance of the WCR for systems having DM-WFS misregistration was not characterized. It is worth noting that while the WCR out-performed the T-Filter reconstructor in this study, the computed Noise Gain in Table 1 for the T-Filter reconstructor is less than that of the WCR. Since, by construction, the WCR is only meant to suppress the waffle mode, it is reasonable to conjecture that when other noise effects are included, the spatial filtering technique may provide less total error propagation than the WCR.

The results presented herein are not unique to the particular AO configuration studied. Other simulations of beam projection systems through horizontal turbulence also showed improvement of the WCR over the Standard reconstructors.

6. REFERENCES

1. Fried, D., Least-square fitting a wave-front distortion estimate to an array of phase-difference measurements, JOSA, vol. 67, no. 3, pp. 370–375, 1977.
2. Makidon, R.B., et. al., Waffle mode error in the AEOS adaptive optics point-spread function, SPIE Proceedings Vol. 4860, 2003.
3. Praus, R.W., II and Venet, B., WaveTrain Adaptive Optics Configuration Guide, MZA Associates Corporation, http://www.mza.com/doc/wavetrain/aogeom/index.htm, 2008.
4. Forsythe, G.E., Malcolm, M.A. and Moler, C.B., *Computer Methods for Mathematical Computations*, Prentice Hall Professional Technical Reference, 1977.
5. Coy, S.C. and Venet, B., WaveTrain User Guide, MZA Associates Corporation, http://www.mza.com/doc/wavetrain/wtug/index.htm, 2011.
6. Spinhirne, J.M., et. al., The Starfire Optical Range 3.5m Telescope Adaptive Optical System, SPIE Vol. 3353, March 1998.
7. Coy, S, et. al., Modeling and Simulation of Beam Control Systems, Short Course Presented at the Seventh Annual Directed Energy Systems Symposium in Rockville, MD, MZA Associates Corporation, 2004.
8. Brennan, T.J., The Use of Spatial Filtering Techniques to Reduce ABL Stability Margin Loss, the Optical Sciences Corporation, April 1999.
9. Garvey, D. et al., Atmospheric Characterization at the HIDL Site, CLEAR I Program, 29 August– 28 September 1984, DR-85-0008; U.S. Army Atmospheric Sciences Laboratory: White Sands Missile Range, NM, 1985.